KYBERNETIKA — VOLUME *46* (2010), NUMBER 2, PAGES 281–293

NUMERICAL SIMULATION OF SUSPENSION INDUCED RHEOLOGY

Rodolphe Prignitz and Eberhard Bänsch

Flow of particles suspended in a fluid can be found in numerous industrial processes utilizing sedimentation, fluidization and lubricated transport such as food processing, catalytic processing, slurries, coating, paper manufacturing, particle injection molding and filter operation. The ability to understand rheology effects of particulate flows is elementary for the design, operation and efficiency of the underlying processes. Despite the fact that particle technology is widely used, it is still an enormous experimental challenge to determine the correct parameters for the process employed. In this paper we present 2-dimensional numerical results for the behavior of a particle based suspension and compare it with analytically results obtained for the Stokes-flow around a single particle.

Keywords: CFD, multiphase flows, particulate flow, finite elements, subspace projection, rheology

Classification: 76D05, 70E55, 76M10

1. INTRODUCTION

The aim of the present paper is to analyze and develop an algorithm for the simulation of a huge amount of particles suspended in a viscous liquid. Related work can be found for instance in [3, 6, 7, 9] and [14]. We adapted the work of [7], such that it fits our requirements to obtain a fast and accurate code for the simulation of a huge number of particles in a viscous fluid. Our own contribution is the representation of the particles utilizing adaptive finite element techniques, the time discretization as well as the incorporation of a subspace projection method. In this paper we report on 2 dimensional simulations, the extension to 3 dimensions is conceptually straightforward and will be published in forthcoming papers. The remainder of the paper is organized as follows. In Section 2 and 3 we present a short overview of the mathematical model and numerical method used, while in Section 4 we present results on the change of rheology in suspended fluids.

2. NUMERICAL METHOD

2.1. Mathematical Model

In this section we introduce a model for particulate flows. For the ease of presentation we restrict ourselves to the $2d$–case with one particle. The extension to $3d$ and/or more particles is straightforward. We denote by $\Omega(t) \subset \mathbb{R}^2$ the area occupied by the fluid with homogeneous Dirichlet boundary condition on its outer boundary Γ_D. $P(t) \subset \mathbb{R}^2$ is the particle and its center of mass is denoted by $X = \frac{1}{|P(t)|} \int_{P(t)} \mathbf{x} \, \mathrm{d}x$,

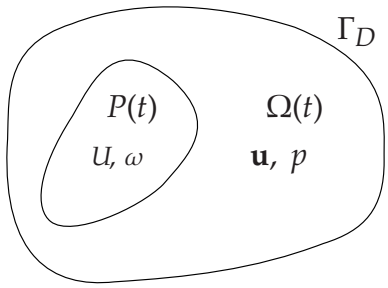

Fig. 1. Fluid domain with arbitrary particle inside.

while $\mathbf{r} = \mathbf{x} - X$ is its relative coordinate. It should be emphasized that the fluid area and the particle area don't intersect, $\Omega(t) \cap P(t) = \emptyset$. The unknowns in the fluid area are the velocity $\mathbf{u}$ and the pressure p, which are described by the Navier–Stokes equations. The particle, being a rigid body, is described by Newton's law. The describing values are the translatorial and angular velocities U, ω, respectively, the position X and the orientation in space given by the angle Θ. The system in non-dimensional form reads

$$\partial_t \mathbf{u} + \mathbf{u} \cdot \nabla \mathbf{u} + \nabla \cdot \overbrace{\left(p\mathbb{I} - \frac{1}{\mathrm{Re}} \mathrm{D}\left[\mathbf{u}\right] \right)}^{\sigma} = f \quad \text{in } \Omega(t), \tag{1}$$

$$\nabla \cdot \mathbf{u} = 0 \quad \text{in } \Omega(t), \tag{2}$$

$$\mathbf{u} = 0 \quad \text{on } \Gamma_D, \tag{3}$$

$$\mathbf{u} = U + \omega \times \mathbf{r} \quad \text{on } \partial P(t), \tag{4}$$

$$M\dot{U} = F + \int_{\partial P(t)} \sigma \cdot \mathbf{n} \, \mathrm{d}s, \tag{5}$$

$$\dot{X} = U, \tag{6}$$

$$I\dot{\omega} = \int_{\partial P(t)} \mathbf{r} \times \sigma \cdot \mathbf{n} \, \mathrm{d}s, \tag{7}$$

$$\dot{\Theta} = \omega, \tag{8}$$

see for example [6]. The two integrals on the right hand side represent the force and the torque, respectively, exerted by the fluid on the particle. Here, σ is the stress

tensor, M denotes the mass of the particle and I its inertia. F is an external force acting on the particle, Re denotes the Reynolds number and the deformation tensor is defined by $\mathrm{D}[\mathbf{u}]_{i,j} = \partial_j u_i + \partial_i u_j$.

Following an idea of [7], we derive a weak formulation of the problem in the form of the *one domain approach*. To this end, the space of combined velocities is defined by

$$H_c(\underline{\Omega}) = \Big\{ (\mathbf{v}, V, \xi) \,|\, \mathbf{v} \in \left(H^1(\underline{\Omega})\right)^2, V \in \mathbb{R}^2, \xi \in \mathbb{R}, \\ \mathbf{v} = 0 \ \text{ on } \Gamma_D, \ \mathbf{v} = V + \xi \times \mathbf{r} \ \text{ in } P(t) \Big\}, \tag{9}$$

where $\xi \times \mathbf{r} := (-r_2\xi, r_1\xi)$. Note that the combined fluid/particle domain $\underline{\Omega} = \Omega(t) \cup P(t)$ does not depend on time t. The space $H_c(\underline{\Omega})$ is called the space of combined velocities, since it contains all velocities posed in this problem, the fluid velocity, the translational particle velocity and the angular velocity represented by $\mathbf{v}$, V and ξ respectively. We emphasize that the fluid velocity is defined on the whole domain $\underline{\Omega}$ and is restricted to the particle velocity inside the particle by the above definition. With test functions $(\mathbf{v}, V, \xi) \in H_c(\underline{\Omega})$ and $q \in L^2(\underline{\Omega})$ we can state the weak formulation of our problem (1)–(8) as

$$\int_{\underline{\Omega}} \partial_t \mathbf{u} \cdot \mathbf{v} + \mathbf{u} \cdot \nabla \mathbf{u} \cdot \mathbf{v} - p \nabla \cdot \mathbf{v} - \frac{1}{2\mathrm{Re}} \mathrm{D}[\mathbf{u}] : \mathrm{D}[\mathbf{v}] \, \mathrm{d}x \\ + (1-\alpha) M \dot{U} \cdot V + (1-\alpha) I \dot{\omega} \cdot \xi = \int_{\underline{\Omega}} f \cdot \mathbf{v} \, \mathrm{d}\mathbf{x} + F \cdot V, \tag{10}$$

$$\int_{\underline{\Omega}} \nabla \cdot \mathbf{u} \, q \, \mathrm{d}x = 0, \tag{11}$$

$$\dot{X} = U, \tag{12}$$

$$\dot{\Theta} = \omega. \tag{13}$$

Hereby α is the density fraction defined by $\alpha = \rho/\rho_P$. In order to obtain this weak formulation one has to perform the symbolic calculation

$$\int_{\Omega(t)} (1) \cdot \mathbf{v} \, \mathrm{d}x + (5) \cdot V + (7) \cdot \xi.$$

After partial integration of the stress tensor term, the boundary integrals arising will cancel with the ones from the terms $(5) \cdot V$ and $(7) \cdot \xi$. Finally the formulation is extended to the domain $\underline{\Omega}$. As we want to focus on the numerical method in the next chapter, we refer the reader to [7] for a more detailed derivation of the weak formulation.

For a shorter notation we define the linear forms

$$m(\mathbf{u}, \mathbf{v}) = \int_{\underline{\Omega}} \mathbf{u} \cdot \mathbf{v} \, \mathrm{d}x, \tag{14}$$

$$s(\mathbf{u},\mathbf{v}) = \frac{1}{2\mathrm{Re}} \int_{\underline{\Omega}} \mathrm{D}\left[\mathbf{u}\right] : \mathrm{D}\left[\mathbf{v}\right] \,\mathrm{d}x, \tag{15}$$

$$k(\mathbf{u},\mathbf{v},\mathbf{w}) = \int_{\underline{\Omega}} \mathbf{w} \cdot \nabla \mathbf{u} \cdot \mathbf{v} \,\mathrm{d}x, \tag{16}$$

$$b(p,\mathbf{v}) = \int_{\underline{\Omega}} p \nabla \cdot \mathbf{v} \,\mathrm{d}x, \tag{17}$$

$$L(U,V) = (1-\alpha) MU \cdot V, \tag{18}$$

$$S(\omega,\xi) = (1-\alpha)\,(I\omega)\cdot\xi, \tag{19}$$

yielding in the following formulation of the problem

$$\begin{aligned} m(\partial_t \mathbf{u},\mathbf{v}) + k(\mathbf{u},\mathbf{v},\mathbf{u}) + s(\mathbf{u},\mathbf{v}) - b(p,\mathbf{v}) + L(\dot{U},V) + S(\dot{\omega},\xi) \\ = m(f,\mathbf{v}) + F\cdot V, \end{aligned} \tag{20}$$

$$b(q,\mathbf{u}) = 0, \tag{21}$$

$$\dot{X} = U, \tag{22}$$

$$\dot{\Theta} = \omega. \tag{23}$$

3. NUMERICAL METHOD

Our numerical scheme to solve the problem (20) – (23) is based on the following four steps

- Splitting: in order to reduce the complexity of the problem we separate the calculation of the particle's time dependent location from the calculation of the flow field.
- Time discretization: a BDF2 projection scheme is used for the efficient solution of the Navier–Stokes equations.
- Subspace projection: a novel method to take into account the restriction of the function space $H_c(\underline{\Omega})$.
- Adaptivity: local (time dependent) grid refinement is crucial to represent the particle's geometry.

3.1. Splitting

For an efficient numerical treatment we initially split the position of the particle from the remaining variables.

1. Predictor: Solve for X, U, Θ, ω using equations (22), (23), $M\dot{U} = F$ and $I\dot{\omega} = 0$.
2. Velocities:

$$\begin{aligned} m(\partial_t \mathbf{u},\mathbf{v}) + k(\mathbf{u},\mathbf{v},\mathbf{u}) + s(\mathbf{u},\mathbf{v}) - b(p,\mathbf{v}) + L(\dot{U},V) + S(\dot{\omega},\xi) = m(f,\mathbf{v}), \\ b(q,\mathbf{u}) = 0. \end{aligned} \tag{24}$$

In the first step the positions $(X,\ \Theta)$ and velocities $(U,\ \omega)$ of the particle are calculated, while in the second step the velocities of the particle are corrected and the fluid velocity and pressure is computed. The effect of the external force F is only taken into account in the predictor step. The force the fluid cause on the particle is created implicitly by the terms $L(\dot{U}, V)$, $S(\dot{\omega}, \xi)$ and the usage of the space of combined velocities $H_c(\underline{\Omega})$.

3.2. Time discretization

For the time discretization of the predictor a *velocity verlet method* with $a = \frac{F}{M}$ for the variables X and U is used:

$$X^{k+1} = X^k + \tau U^k + \frac{\tau^2}{2} a^k, \tag{25}$$

$$U^{k+\frac{1}{2}} = U^k + \frac{\tau}{2} a^k, \tag{26}$$

$$a^{k+1} = \text{evaluate forces at new positions } X^{k+1}, \tag{27}$$

$$U^{k+1} = U^{k+\frac{1}{2}} + \frac{\tau}{2} a^{k+1}. \tag{28}$$

For a more detailed description of the algorithm see for example [11]. The same is valid for the variables Θ and ω.

The flow field governed by the Navier–Stokes equations is solved by a BDF2 based projection method in rotational form, see [8]. Introducing the time step τ, and $\gamma = \frac{2}{3}\tau$ this scheme is based on three steps to solve equations (24):

1. Burgers problem

$$\begin{aligned} m(\mathbf{u}^{k+1}, \mathbf{v}) &+ \gamma k(\mathbf{u}^{k+1}, \mathbf{v}, \mathbf{u}^{k+1}) + \gamma s(\mathbf{u}^{k+1}, \mathbf{v}) \\ &+ \frac{2}{3} L(U^{k+1}, V) + \frac{2}{3} S(\omega^{k+1}, \xi) \\ &= \gamma b(p^k, \mathbf{v}) + \gamma m(f(t^{k+1}), \mathbf{v}) \\ &+ m\left(\frac{4}{3}\mathbf{u}^k - \frac{1}{3}\mathbf{u}^{k-1}, \mathbf{v}\right) + \gamma b\left(\frac{4}{3}\chi^k - \frac{1}{3}\chi^{k-1}, \mathbf{v}\right) \\ &+ \frac{2}{3} L(U^k, V) + \frac{2}{3} S(\omega^k, \xi). \end{aligned} \tag{29}$$

2. Poisson problem

$$m(\nabla\chi^{k+1}, \nabla\Psi) = \frac{1}{\gamma} b(\Psi, \mathbf{u}^{k+1}). \tag{30}$$

3. Update

$$m(p^{k+1}, q) = m(p^k + \chi^{k+1}, q) - b\left(q, \frac{2}{\mathrm{Re}}\mathbf{u}^{k+1}\right). \tag{31}$$

In the calculations presented later, the form k is linearized by $k(\mathbf{u}^{k+1}, \mathbf{v}, 2\mathbf{u}^k - \mathbf{u}^{k-1})$.

3.3. Spatial discretization

The crucial point in the spatial discretization is to define a discrete counterpart of $H_c(\underline{\Omega})$ and, moreover, the concrete realization of the this non-standard finite element space. A brief description of how to solve this problem is given in the sequel. A more detailed presentation will be published in near future.

Let $\mathcal{T}$ be a triangulation of $\underline{\Omega}$. Define the usual finite element space by

$$X(\underline{\Omega}) = \Big\{ (\mathbf{v}, V, \xi) \,|\, \mathbf{v} \in \left(C^0(\underline{\Omega})\right)^2, \, \mathbf{v} \in \left(P^k(T)\right)^2 \forall\, T \in \mathcal{T}, \\ V \in \mathbb{R}^2, \, \xi \in \mathbb{R}, \mathbf{v} = 0 \ \text{ on } \Gamma_D \Big\}.$$

A discrete subspace of $H_c(\underline{\Omega})$ is now given by

$$X_c(\underline{\Omega}) = \Big\{ (\mathbf{v}_c, V, \xi) \in X(\underline{\Omega}) |\ \mathbf{v}_c = V + \xi \times \mathbf{r} \ \text{ in } P(t) \Big\}.$$

For an arbitrary time step k the linearized equation (29) may be rewritten with the bilinear form a, the corresponding operator $\mathcal{A}$, and the cumulative right hand side g: find $\mathbf{u} \in X_c(\underline{\Omega})$ such that for all $\mathbf{v} \in X_c(\underline{\Omega})$ it holds

$$a(\mathbf{u}, \mathbf{v}) =: (\mathcal{A}\mathbf{u}, \mathbf{v}) = (g, \mathbf{v}). \tag{32}$$

To circumvent the explicit representation of $H_c(\underline{\Omega})$, a subspace projection $\mathcal{P} : X \to X_c$ is used. With this operator (32) may be formulated in terms of the *standard* finite element space $X(\underline{\Omega})$: find $\tilde{\mathbf{u}} \in X(\underline{\Omega})$ such that for all $\mathbf{v} \in X(\underline{\Omega})$ it holds

$$(\mathcal{A}\mathcal{P}\tilde{\mathbf{u}}, \mathcal{P}\mathbf{v}) = (g, \mathcal{P}\mathbf{v}). \tag{33}$$

Note that the solution $\mathbf{u}$ is now easily found by taking $\mathbf{u} = \mathcal{P}\tilde{\mathbf{u}}$, where $\tilde{\mathbf{u}}$ is a solution of equation (33). The above system now leads to the linear system of equations for the nodal vector $\tilde{U}$ of the form

$$P^T A P \tilde{U} = P^T G, \tag{34}$$

where A is the system matrix corresponding to operator $\mathcal{A}$ and P is a matrix representation of $\mathcal{P}$. Note that, when using iterative solvers, one can bypass to explicitly compute the modified system matrix $P^T AP$, but rather just slightly needs to modify the matrix vector product, because one only has to take into account the action of $P^T AP$ on a vector. We call this method subspace projection method. Because the matrix P is quite simple, its not necessary to store it explicitly. Instead, a short routine can perform the multiplication of P and P^T with a vector $\mathbf{v}$. This pseudo-code shows that computation.

```
! Multiplication (u,U,omega)=P*(v,V,xi)
subroutine Pmul(v,V,xi,u,U,omega)

   ! U, omega
   do ii=1,npart ! Number of particles
      U(:,ii)    = V(:,ii)
      omega(ii)  = xi(ii)
   end do

   ! u = rigid body motion in the particle
   do i=1,nk ! Number of DOFs
      if( isparticle(i) ) then
         ii= numpart(i)
         r(:)= x(:,i) - xpart(:,ii)
         u(1,i) = V(1,ii) - r(2)*xi(ii)
         u(2,i) = V(2,ii) + r(1)*xi(ii)
      else
         u(:,i)= v(:,i)
      end if
   end do

end subroutine
```

3.4. Adaptivity

Another important point is how to represent the particle's geometry. In [9] a remeshing technique was used to explicitly follow the geometry in time, [14] introduced a mesh deformation technique and [7] used Lagrange multipliers. All these techniques have some pros and cons, in particular in 3d.

In contrast to the above mentioned methods, we use time dependent adaptively refined grids based on the bisection method by [1] to sufficiently resolve the region around the particle.

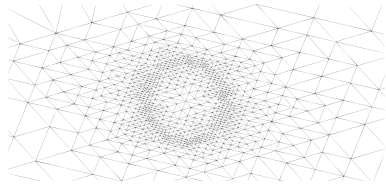

Fig. 2. Adaptive refined mesh around a particle. For an accurate representation it is useful to refine the mesh on the particle boundary.

The above algorithm was implemented in the finite element flow solver NAVIER, for more details see [2].

4. APPLICATION

4.1. Sedimentation

The first test case presented here is the sedimentation of a single particle in a lighter fluid. Though conceptually rather simple, this test case might be already quite revealing. Here, the quantity of interest is the terminal particle velocity, denoted by U and the corresponding drag c_D defined by

$$F = \frac{1}{2}\rho c_D \, \mathrm{d} U^2. \tag{35}$$

Let us mention that, unlike the 3d case, it is rather difficult to get reliable data for the validation. We compared the drag coefficient with experimental data by [13], numerical data by [6] and semi-analytical results from [12], resulting in a pretty good agreement, see Figure 3. It is worth noting that care must be taken regarding wall effects. This can be clearly seen in Figure 3, where curves for different values of the ratio l/d are plotted. Here, d is the particle's diameter and l the diameter of the fluid domain. For low Reynolds numbers $\mathrm{Re} = \frac{dU}{\nu}$, where large wall friction is present, a small ratio l/d produces results that are far off the desired ones.

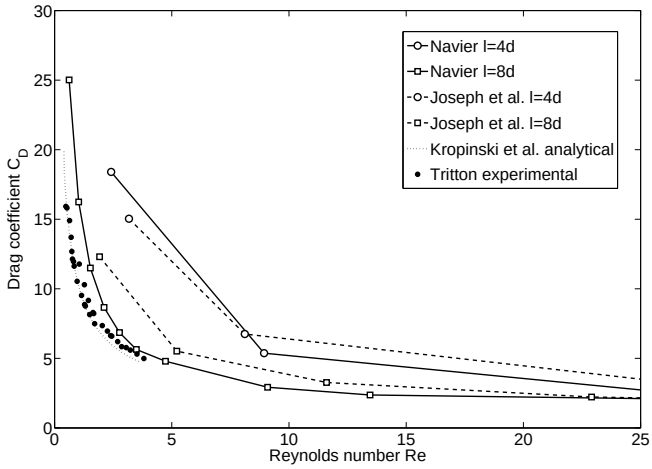

Fig. 3. Comparison of drag curves.

4.2. Rotational viscometer

In order to study the rheology of suspended liquids, a rotational viscometer is simulated. This is a device to measure the viscosity of fluids by applying a forced rotational flow field. The fluid is confined between two concentric cylinders. The outer one is called cup, the inner one bob, see Figure 4. By rotating the cup and

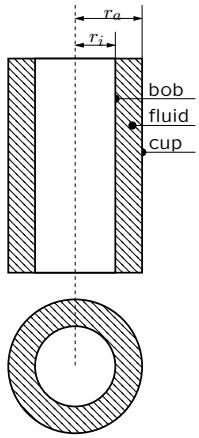

Fig. 4. Rotational viscometer.

measuring the required torque, one can calculate the viscosity of the fluid. A short calculation shows that as long as the flow field is stable, the (non-dimensional) form of the flow field is independent of the rotational speed o. Assuming the shear rate to be approximately constant, it can be calculated from the rotational speed o by

$$\frac{\mathrm{d}u_\varphi}{\mathrm{d}r} = \frac{2\pi r_a o}{r_a - r_i}, \tag{36}$$

where r_i, r_a denote the inner and outer radii, respectively, and u_φ the azimuthal component of $\mathbf{u}$. The shear stress τ on the surface is given by the torque T through

$$\tau = \frac{T}{2\pi r_a^2}. \tag{37}$$

Finally the viscosity is calculated by

$$\eta = \frac{T(r_a - r_i)}{4\pi^2 o r_a^3}. \tag{38}$$

Consequently, in a rotational viscometer the viscosity of the fluid is proportional to the measured torque. Define the relative viscosity $\eta^\blacklozenge$ by

$$\eta^\blacklozenge = \frac{\eta_{\mathrm{eff}}}{\eta} = \frac{T_{\mathrm{eff}}}{T}, \tag{39}$$

where η_{eff} is the effective viscosity of the suspension measured in our numerical experiments and η the viscosity of the fluid. The torque T is calculated by evaluating the integral $\int_{\partial B(0,r_a)} \mathbf{x} \times \sigma \cdot \mathbf{n}\,\mathrm{d}s$ numerically. The computational experiments were performed with two different particle radii, $r = 0.02$ and $r = 0.04$ see Figure 6 for a visualization of such computations. For the smaller one calculations were conducted for particle volume fractions ϕ up to 40 %, for the larger one up to 20 %. The results

in Figure 5 show a linear behavior of the relative viscosity up to 20 % of particle volume fraction. For larger ϕ the relative viscosity increases super linearly. In addition, there is no influence of the particle size in the results. The same qualitative characteristics can be observed in 3d-experiments, see for example the overview article by [10]. A linear fit for low values of ϕ suggests a behavior like

$$\eta^{\blacklozenge} = \eta\,(1 + 1.77\phi)\,. \tag{40}$$

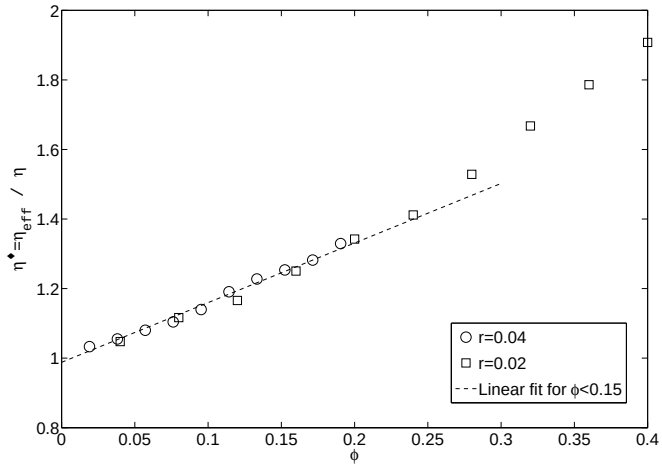

Fig. 5. Numerical results of relative viscosity versus particle concentration.

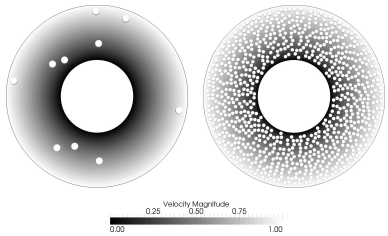

Fig. 6. Visualization of simulations with 10 particles of radius $r = 0.04$ (left) and 840 particles with radius $r = 0.02$ (right).

To support our calculations we derived an analytical solution following the approach in [5]. To this end, a single particle suspended in a steady shear flow $\mathbf{u} = (u, v) = (Cy, 0)$ is considered. Furthermore, the flow is assumed to be governed by the Stokes equations

$$-\eta\Delta\mathbf{u} + \nabla p = 0, \qquad \nabla\cdot\mathbf{u} = 0, \qquad \mathbf{u} = 0 \ \text{ on } \partial P. \tag{41}$$

With help from [4] the following solution is found:

$$u = Cy - \frac{1}{2}\frac{CR^2 y}{x^2+y^2} - 2\frac{CR^2 yx^2}{\left(x^2+y^2\right)^2} - \frac{1}{4}CR^4\left(2\frac{y}{\left(x^2+y^2\right)^2} - 8\frac{x^2 y}{\left(x^2+y^2\right)^3}\right), \quad (42)$$

$$v = \frac{1}{2}\frac{CR^2 x}{x^2+y^2} - 2\frac{CR^2 y^2 x}{\left(x^2+y^2\right)^2} - \frac{1}{4}CR^4\left(-8\frac{y^2 x}{\left(x^2+y^2\right)^3} + 2\frac{x}{\left(x^2+y^2\right)^2}\right), \quad (43)$$

$$p = -4\eta\frac{CR^2 yx}{\left(x^2+y^2\right)^2} \quad (44)$$

with the particle radius R. The amount of energy dissipated in a very large circular domain $B(0,Q)$ of radius $Q \gg R$ is then given by

$$W = \int_{\partial B(0,Q)} \sigma\cdot\mathbf{u}\,\mathrm{d}s = C^2\eta\pi\,Q^2 + C^2\eta\pi\,R^2 - 5\frac{C^2 k\pi\,R^4}{Q^2} + 6\frac{C^2 k\pi\,R^6}{Q^4} - 3\frac{C^2\eta\pi\,R^8}{Q^6}, \quad (45)$$

while the loss of energy due to friction of the *unperturbed* flow $\mathbf{u} = (Cy, 0)$ in the same domain is

$$W_{\mathbf{u}} = C^2\eta\pi\,Q^2. \quad (46)$$

If terms of order $1/Q^2$ or greater are ignored in equation (45), one obtain

$$\triangle W = W - W_{\mathbf{u}} = C^2\eta\pi\,R^2 = \eta C^2\Phi \quad (47)$$

for the energy loss caused by one particle with area $\Phi = \pi R^2$. If we assume a sparse distribution of n particles in the fluid domain with area πQ^2 the overall specific energy loss is

$$w := \frac{W}{\pi Q^2} = \eta C^2 + \eta\frac{C^2}{\pi Q^2}\sum^{n}\Phi = \eta C^2\left(1+\phi\right), \quad (48)$$

with $\phi = n\Phi$. On the other hand, the specific energy loss of the suspension is

$$w = C^{\blacklozenge 2}\eta^{\blacklozenge}. \quad (49)$$

$C^{\blacklozenge}$ can be calculated from the solutions (42) – (44) of the Stokes problem, resulting in

$$C^{\blacklozenge} = C - n\int_{\partial B(0,Q)}\frac{(u-Cy)\,y}{\sqrt{x^2+y^2}}\,\mathrm{d}s = C - nC\pi R^2 = C\left(1-\phi\right). \quad (50)$$

Inserting equations (48) and (50) into (49) finally yields

$$\eta^{\blacklozenge} = \eta\frac{1+\phi}{\left(1-\phi\right)^2} \approx \eta\left(1+3\phi\right). \quad (51)$$

This theoretical finding is of the same order of magnitude like the one from our computational result:

$$\eta^{\blacklozenge}_{\mathrm{num}} \approx \eta\left(1+1.77\phi\right). \quad (52)$$

Quantitatively, however, there is quite a noticeable discrepancy. A possible reason might be the use of Stokes flow instead of for instance Oseen flow. For Oseen flow, to our knowledge, there is no explicit solution available though. Thus, this problem remains open and deserves further investigation. In the three dimensional case, analytical as well as experimental results are more accessible. It is known, that in this case the above relation reads

$$\eta^{\blacklozenge} \approx \eta\,(1 + 2.5\phi)\,. \tag{53}$$

5. CONCLUSION

In this paper a finite element method to compute particular flow was presented. The methods is based on a weak formulation in the form of a *one domain approach*, a splitting scheme in time, adaptive grids and a subspace projection method.

A validation with a sedimenting particle results in good agreement to experimental and theoretical results. For the case of a rotational viscometer good qualitative agreement is found with a analytical consideration. However, quantitatively there is a non negligible discrepancy, which makes further investigation, in particular 3d simulation, necessary.

ACKNOWLEDGMENT

This work was supported by the Bayerische Forschungsstiftung, which is gratefully acknowledged.

(Received March 3, 2010)

REFERENCES

[1] E. Bänsch: Local mesh refinement in 2 and 3 dimensions. IMPACT Comput. Sci. Engrg. *3* (1991), 181–191. doi10.1016/0899-8248(91)90006-G.

[2] E. Bänsch: Simulation of instationary, incompressible flows. Acta Math. Univ. Comenian. *67* (1997), 1, 101–114.

[3] S. Bönisch and V. Heuveline: On the numerical simulation of the instationary free fall of a solid in a fluid. 1. The Newtonian case. Comput. Fluids *36* (2007), 1434–1445.

[4] A. T. Chwang and T. Yao-Tsu Wu: Hydromechanics of low-reynolds-number flow. Part 2. Singularity method for stokes flows. J. Fluid Mech. *67* (1975), 787–815.

[5] A. Einstein: Untersuchungen über die Theorie der Brownschen Bewegung. Verlag Harri Deutsch, 1905.

[6] J. Feng, H. H. Hu, and D. D. Joseph: Direct simulation of initial value problems for the motion of solid bodies in a newtonian fluid. Part 1. Sedimentation. J. Fluid Mech. *261* (1994), 95–134.

[7] R. Glowinski, T.-W. Pan, T. I. Hesla, and D. D. Joseph: A distributed lagrange multiplier/fictitious domain method for particulate flows. Internat. J. Multiphase Flow *25* (1999), 755–794. doi10.1016/S0301-9322(98)00048-2.

[8] J. L. Guermond and J. Shen: On the error estimates for the rotational pressure-correction projection methods. Math. Comp. *73* (2004), 1719–1737.

[9] H. H. Hu: Direct simulation of flows of solid-liquid mixtures. Internat. J. Multiphase Flow *22* (1996), 2, 335–352.

[10] D. J. Jeffrey and A. Acrivos: The rheological properties of suspensions of rigid particles. AIChe J. *22* (1976), 417–432.

[11] N. S. Martys and R. D. Mountain: Velocity Verlet algorithm for dissipative-particle-dynamics-based models of suspensions. Phys. Rev. E *59* (1999), 3, 3733–3736.

[12] M. S. Titcombe, M. J. Ward, and M. C. Kropinski: A hybrid method for low reynolds number flow past an asymmetric cylindrical body. SIAM J. Appl. Math. *55* (1994), 1484–1510.

[13] D. J. Tritton: Experiments on the flow past a circular cylinder at low reynolds numbers. J. Fluid Mech. *6* (1959), 547–567.

[14] D. Wan and S. Turek: Fictitious boundary and moving mesh methods for the numerical simulation of rigid particulate flows. J. Comput. Phys. *222* (2007), 28–56.

Rodolphe Prignitz, Chair of Applied Mathematics 3, Haberstr. 2, 91058 Erlangen. Germany.

e-mail: prignitz@am.uni-erlangen.de

Eberhard Bänsch, Chair of Applied Mathematics 3, Haberstr. 2, 91058 Erlangen. Germany.

e-mail: baensch@am.uni-erlangen.de